Combining Fluorescence Lifetime and Polarization Microscopy to Discriminate Phase Separated Domains in Giant Unilamellar Vesicles

Christopher K. Haluska,* André P. Schröder,* Pascal Didier,† Denis Heissler,‡ Guy Duportail,† Yves Mély,† and Carlos M. Marques*

*Université Louis Pasteur, Institut Charles Sadron, CNRS UPR 022, Strasbourg, France; †Institut Gilbert Laustriat, CNRS UMR 7175, Laboratoire de Pharmacologie et Physicochimie, Université Louis Pasteur, Illkirch, France; and ‡Institut de Chimie, CNRS UMR 7177, Université Louis Pasteur, Strasbourg, France

ABSTRACT Using fluorescence lifetime microscopy we study the structure of lipid domains in giant unilamellar vesicles made from sphingomyelin, 1,2-dioleoyl-*sn*-glycero-3-phosphocholine, and cholesterol. Lifetimes and orientation of a derivative of the fluorescent probe DPH embedded in the membrane were measured for binary and ternary lipid mixtures incorporating up to 42 mol % of cholesterol. The results show that adding cholesterol always increases the lifetime of the probe studied. In addition, the analysis of the probe orientation indicates that cholesterol has little influence on the ordering of the sphingomyelin alkyl chains whereas it has a noticeable effect on the structure of the 1,2-dioleoyl-*sn*-glycero-3-phosphocholine chains. The measurements made on the orientation and lifetime of the probe show the structure of the membrane in its liquid ordered and liquid disordered domains.

INTRODUCTION

Giant unilamellar vesicles (GUVs) made from ternary mixtures of 1,2-dioleoyl-*sn*-glycero-3-phosphocholine (DOPC), sphingomyelin (SM), and cholesterol are believed to be the most relevant biomimetic systems for understanding the formation of lipid rafts in cellular membranes (1,2). In biological membranes, the so-called, lipid rafts are presumed to exist as membrane microdomains enriched in the liquid-ordered (L_o) phase resulting from packing of the long saturated alkyl chains of sphingolipids and cholesterol, and segregating from the liquid-disordered (L_d) phase composed of unsaturated phospholipids (3). The importance of these domains for cellular functions was first put forward by Simons and Ikonen (4), who suggested that the lipid rafts play a key role in trafficking and signaling in the cell by providing a favorable membrane environment for protein binding. This raft hypothesis has prompted numerous studies in the phase separation of various lipid mixtures in bilayers (5,6).

Domain formation in the lipid bilayers of GUVs occurs in the presence of at least two types of lipids with significantly different phase behavior (7). For instance, vesicles made from unsaturated glycerophospholipid DOPC are in the fluid phase at room temperature, whereas vesicles made from saturated sphingomyelin (SM) are in the gel phase. Two-component membranes made from these two lipids show coexistence of gel and fluid domains. Addition of cholesterol to the mixture significantly changes the structure of the domains. SM domains enriched with cholesterol, identical to lipid rafts, are usually referred to as being in the liquid ordered phase, whereas mixtures of cholesterol with DOPC are in the liquid disordered phase (6).

Although many different techniques can be used to identify phase separation in phospholipid mixtures, the characterization of segregated domains on giant vesicles has been greatly facilitated by the use of fluorescence microscopy techniques (8). The identification of the different domains is made possible by the preferential partitioning of fluorescent probes into L_o and L_d phases (9–11). This has allowed the construction of triangular phase diagrams showing the regions of two-phase coexistence between L_o and L_d phases (12–14). The characterization of the structure and composition of the individual domains is, however, more difficult to achieve. Information on the local environment surrounding a probe in the membrane can be obtained by studying the average polarization and fluorescence lifetime of suspensions of small vesicles (15), or the polarization and fluorescence lifetimes of individual giant vesicles with modified optical microscopes (16–20).

In this study, we carried out two-photon fluorescence microscopy on GUVs of ternary compositions to extract local information on the structure and composition of their domains. For this purpose, we labeled the vesicles with a long chain derivative of diphenylhexatriene (DPH), LcTMA-DPH. The fluorescent probe LcTMA-DPH, has a total length of ~50 Å with its rod-like DPH fluorophore at the end of the long carbon chain, as depicted in Fig. 1, which has been shown to partition preferentially into gel and liquid ordered phases (21) and has already been used as a raft marker (22,23). We implemented fluorescence lifetime imaging microscopy (FLIM), and by taking advantage of the linearly polarized excitation beam, polarization imaging microscopy. We present the data obtained from over 150 different GUVs for 12 different lipid mixtures within the DOPC-SM-cholesterol ternary phase diagram. The measurements allow us to determine

Submitted February 25, 2008, and accepted for publication August 6, 2008.

Address reprint requests to Christopher K Haluska, Institut Charles Sadron, Membranes and Microforces, 23 rue du Loess, CNRS-UPR 22, BP 84047, Strasbourg F-67034, France. Tel.: 33-388-414 000; E-mail: haluska@ics.u-strasbg.fr.

Editor: Thomas J. McIntosh.

0006-3495/08/12/5737/11 $2.00

doi: 10.1529/biophysj.108.131490

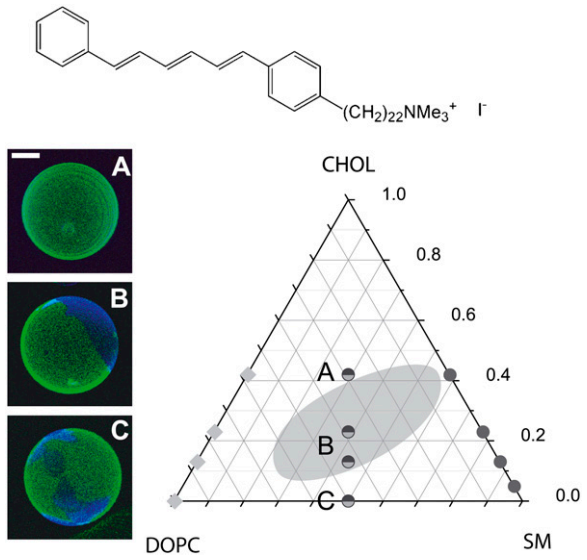

FIGURE 1 Confocal microscopy images of GUVs made from SM and DOPC (1:1) containing different mole fractions of cholesterol, either (*A*) $X_{Ch} = 0.42$; (*B*) $X_{Ch} = 0.13$; or (*C*) $X_{Ch} = 0.0$, and their location in the miscibility phase diagram (scale bar = 10 μm). The phase diagram indicates the lipid composition of the vesicles and where phase separation is known to occur at room temperature (*shaded region*). The chemical structure of the blue probe used in this study is also shown.

the values of the order parameters (*S*,*P*) and of the fluorescence lifetime (τ) based on the composition of the vesicle bilayer.

MATERIALS AND METHODS

Lipids and membrane mixtures

The lipids used in this study were DOPC (Avanti Polar Lipids, Alabaster, AL), *N*-acyl-D-sphingosine-1-phosphocholine from bovine brain, i.e., sphingomyelin (SM) (Sigma-Aldrich, Lyon, France), and cholesterol (Ch) (Sigma-Aldrich). Bovine brain sphingomyelin presents a 70% saturated fatty acids distribution, essentially stearic acid or higher, and a saturation index (S/U) of 3.5. The lipid mixtures used to make the vesicles were based on: DOPC, with four different molar fractions of cholesterol, $X_{Ch} = 0.0$, 0.13, 0.23, 0.42; SM, with four different molar fractions of cholesterol, $X_{Ch} = 0.05$, 0.13, 0.23, 0.42; or an equimolar ratio of SM and DOPC with four different molar fractions of cholesterol, $X_{Ch} = 0.0$, 0.13, 0.23, 0.42.

Fluorescent probes

Two fluorescent probes, emitting in the blue and in the green, were used to label the vesicles. The blue-emitting dye, 22-(diphenylhexatrienyl)-docosyltrimethylammonium (LcTMA-DPH), was synthesized as described (24) and used in the FLIM measurements, whereas the green-emitting dye, (1,2-dioleoyl-*sn*-glycero-3-phosphoethanolamine-*N*-(7-nitro-2-1,3-benzoxadiazol-4-yl)) (NBD-DOPE), a headgroup-labeled unsaturated phospholipid from Avanti Polar Lipids, was used for general imaging and visualization of the fluid domains. The total mole fraction of fluorescent probes never exceeded $X_{probe} = 0.001$ of the total lipid content.

Giant vesicles

Giant unilamellar vesicles were produced using the electroformation technique (25). Two microliters of a given lipid mixture was spread as a thin film on a single piece of indium tin oxide (ITO) glass. This piece of glass was then placed in a desiccator for at least 2 h to remove any traces of chloroform from the lipid film. A complementary piece of ITO glass was placed opposite, and separated from the glass with the lipid film by a 2 mm thick Teflon spacer. The chamber was sealed with silicone grease. A 200 mM sucrose solution was used to fill the chamber. The electroformation chamber was then placed in an oven at 60°C and the voltage was ramped up from 1 V_{rms} to 2 V_{rms} over a 2 h period. The vesicle solution was then collected and placed in an Eppendorf tube. After 12 h, this solution was mixed with an isotonic glucose solution.

FLIM measurements

All measurements were carried out at 20°C on a homemade two-photon laser scanning microscope based on the setup described previously (26). Excitation light was generated using a mode-locked Ti:SAPHIRE laser (Spectra-Physics, Mountain View, CA) operating at a repetition rate of 82 MHz and tuned to 750 nm. Scanning and imaging were carried out using galvomirrors at a speed rate of 1 s per frame (50×50 μm^2) and with an excitation power of 4 mW at the level of the sample. The emitted fluorescence from the sample was descanned and filtered through a 700SP filter (Coherent, Santa Clara, CA) to reject residual excitation laser light. The fluorescence was detected by a photon-counting module (Perkin-Elmer Optoelectronics, Fremont, CA) and the signal sent to a SPC830 time-correlated single-photon counting card (Becker and Hickl GMBH, Berlin, Germany) used in the fluorescence lifetime imaging mode. Image acquisition times were typically 120 s depending on the intensity of the fluorescence signal. The minimum and maximum photon counts per pixel were on the order of 10^2–10^5, respectively.

The data were analyzed using a commercial software package (SPCImage V2.9; Becker and Hickl), which uses an iterative reconvolution method to recover the lifetimes from the fluorescence decays. Due to the uniformity of the membrane mixtures, a mono-exponential curve was used to fit the fluorescence decay for each individual group of binned pixels (binning was set to 3). A corresponding fluorescence lifetime histogram that accounts for the whole image was generated for each acquisition. Fluorescence decays near the vesicle poles, where intensity was the lowest, produced artificially low fluorescence lifetimes due to poor photon statistics. To obtain reliable lifetime histograms the region of interest was then limited to pixels groups with a photon number >100. The histograms displayed in the figures were obtained by summing up to 25 individual GUV histograms for a particular membrane mixture.

Measuring the influence of probe orientation

Information on the degree of orientation of the probe in the membrane was extracted from the variation of the intensity, $I(\theta)$, with the angle θ measured clockwise around the vesicle contour. Values for $I(\theta)$ were obtained by dividing a given contour into at least 256 sectors, and by summing the intensity originated from the contour inside each angular sector. The experimental data were then fitted using the function

$$I(\theta) = A(1/5 - 2S/7 + 3P/35 + 6(S - P)/7 \sin^2(\theta) + P \sin^4(\theta)). \quad (1)$$

The fit provides two order parameters, *S* and *P*, which correspond to different moments of the probe orientation distribution, as further detailed in the Appendix and in the Discussion section below, and *A* is a constant reflecting total intensity.

RESULTS

The simplified phase diagram of the system studied in this study is shown in Fig. 1. In the diagram, the bottom left

corner corresponds to a pure DOPC vesicle whereas the bottom right corner represents a pure SM vesicle. The vertical axis indicates the molar fraction of cholesterol in the DOPC-SM mixed vesicles. Phase separation occurs in the central region of this phase diagram, whereas gel phase domains in the SM/DOPC binary systems are observed for vesicle compositions along the bottom of the triangle (14,27). Note that minor differences between the phase diagrams in different studies might be due to the nature of the SM tail distribution, in particular in lipid mixtures containing low cholesterol content. We chose to explore the structure of the bilayer formed from ternary mixtures, with an equimolar DOPC/SM ratio and four different molar fractions of cholesterol (X_{Ch}): 0, 0.13, 0.23, and 0.42, which are positioned along the vertical median line of the phase diagram. For reference, we also analyzed the corresponding GUVs made from binary mixtures, made either from DOPC or SM, and similar molar fractions of cholesterol as used in the ternary systems. The composition of these samples is displayed along the two sides of the triangular phase diagram (Fig. 1). Note that due to practical reasons for the electroformation of giant vesicles from a pure gel phase lipid, we chose to study SM vesicles with a minimum of 0.05 molar fraction of cholesterol rather than vesicles composed solely from SM. Of 12 compositions studied, the two on the median line at 0.13 and 0.23 cholesterol molar fraction are located in a region of two-phase coexistence. In these cases, at equilibrium, the bilayer is segregated completely into two domains; one corresponding to the liquid ordered phase (L_o), and the other one to the liquid disordered phase (L_d). The lipid mixture on the median line, at zero cholesterol content, also displays phase separation between the gel and fluid phases of the two different lipids. All the other compositions correspond to homogeneous mixtures of lipids, at least for dimensions above the optical resolution of the microscope ($\sim$0.5 μm). To illustrate the typical differences between homogeneous and phase separated vesicles, we show 3D micrographs of vesicles reconstituted from *z*-stacks obtained by using laser scanning confocal microscopy (Fig. 1, *A–C insets*).

Visualization of the different phases was achieved with the blue-emitting probe LcTMA-DPH that preferentially partitions into gel and L_o phases (21), and with the green-emitting probe NBD-DOPE that preferentially partitions into fluid phases, including the L_d phase. Fig. 1, *inset A*, displays a vesicle (SM/DOPC 1:1, $X_{Ch} = 0.42$) with a homogeneous distribution of phospholipids. The vesicle contains both green and blue probes distributed homogeneously throughout the vesicle, only the green probe is displayed for clarity. Fig. 1, *inset B*, displays a typical image for a vesicle (SM/DOPC 1:1, $X_{Ch} = 0.13$) with coexisting L_o and L_d phases, with domain sizes comparable to the vesicle radius. An example of coexistence between the liquid phase (DOPC) and gel phase (SM) domains is shown in Fig. 1, *inset C*, for a vesicle made from SM and DOPC 1:1 in the absence of cholesterol. In particular, care was taken to allow enough time for completion of the phase separation between the different domains so that all images were taken at equilibrium. Note that the NBD-DOPE-labeled lipid was only used for the purpose of illustration (i.e., in Fig. 1), and that all lifetime and polarization results that will be described were obtained from GUVs that contained only LcTMA-DPH as fluorescent probe.

The effect of cholesterol on the structure of the DOPC based GUVs is displayed in Fig. 2. Fig. 2, *A–D*, shows two sets of images obtained using the FLIM setup for each of the four bilayer compositions analyzed: $X_{Ch} = 0.00$, 0.13, 0.23, and 0.42. The top row shows falsely colored fluorescence lifetime images, and the bottom row shows the corresponding fluorescence intensity images. Experiments were carried out on at least 10 vesicles for each composition. One can see the variation in fluorescence lifetime in the first row of FLIM images based on membrane cholesterol concentration, blue coloration representing shorter, and yellow representing longer, fluorescence lifetimes on the color spectrum. The fluorescence lifetime color spectrum in the micrographs is identical to the one presented in the lifetime axis (τ) of the cumulative lifetime histograms (Fig. 2 *G*). It should be noted that the FLIM images shown only contribute to a small portion of the overall cumulative lifetime histogram, which is compiled from measurements made on a number of different GUVs. Note that we present only the falsely colored fluorescence lifetime images in Fig. 2 because the variation in mean fluorescence lifetime based on the composition of the membrane is more accurately represented and recognized in a comparison of the lifetime histograms. Another striking feature shown in the bottom row of Fig. 2, *A–D*, is the variation of the fluorescence intensity clockwise around the vesicle contour in the equatorial plane. Because the typical acquisition time of each FLIM measurement was 120 s, the intensity mainly reflects the equilibrium distribution of the LcTMA-DPH probe with respect to the axis of polarized excitation light (28).

As explained in the Appendix, it is known that the expected intensity distribution for the probe in the membrane, $I(\theta)$, follows Eq. 1, which is comprised of a constant term plus quadratic, $\sin^2(\theta)$, and quartic, $\sin^4(\theta)$, terms (29–31) where θ is the equatorial angle with respect to the polarization axis. Furthermore, if α is the angle of the probe with respect to the membrane normal, and $g(\alpha)$ is the equilibrium distribution of the probe orientation, one defines order parameters, S and P, for the probe as, $S = \langle(3\cos(\alpha)^2 - 1)/2\rangle$, and $P = \langle(3 - 30\cos(\alpha)^2 + 35\cos(\alpha)^4)/8\rangle$. The average $\langle\ \rangle$ is measured with the probability distribution $g(\alpha)$. A value of the order parameter, S, close to unity indicates strong confinement of the orientational degrees of freedom of the probe in the direction of the normal to the membrane. On the other hand, a completely isotropic angular distribution $g(\alpha) = 0.5$, leads to S values close to zero. Information provided by the fourth order moment, P, will be analyzed in the Discussion section below. Fig. 2 *E* shows four typical $I(\theta)$ curves from the four

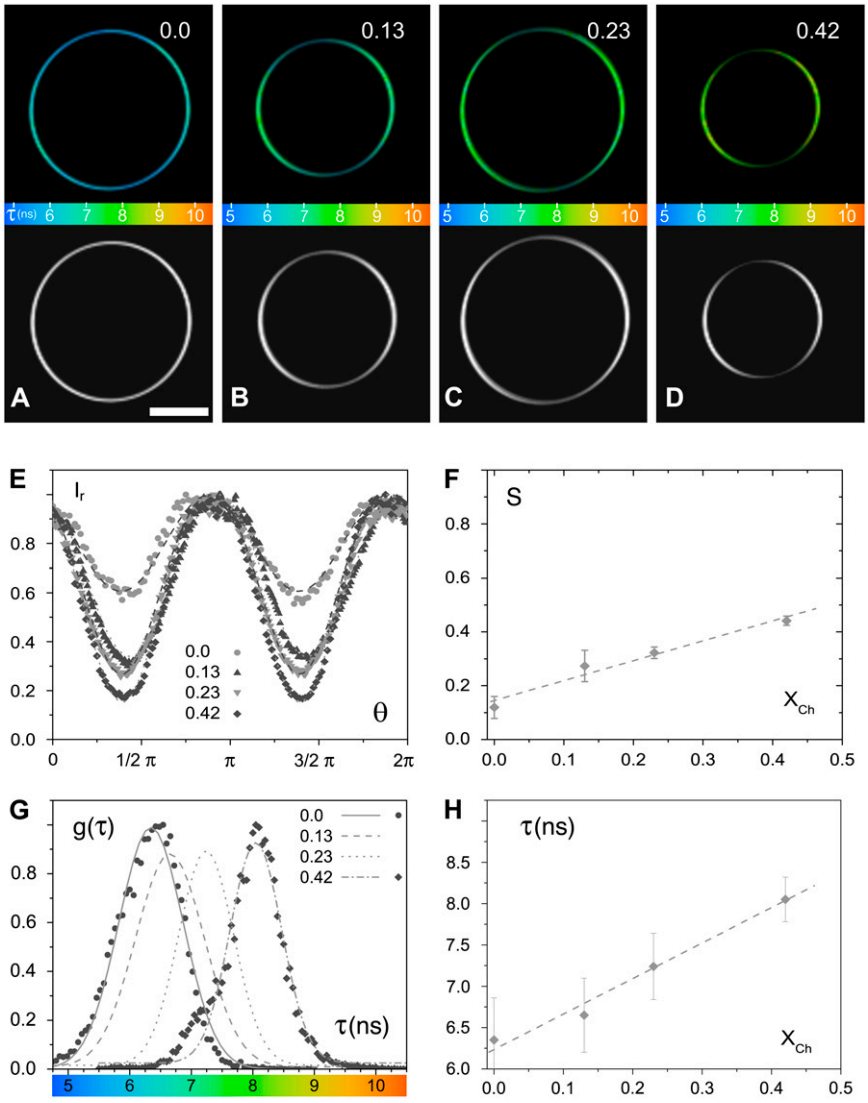

FIGURE 2 (*A–D*) The two rows of micrographs include four FLIM images, where the pixels contain information based on the fluorescence lifetimes measured for a given vesicle (*top*), and the corresponding FLIM intensity images (*bottom*) representative of GUVs made from binary mixtures of DOPC and cholesterol. The numbers refer to the mole fraction of cholesterol (X_{Ch}) in a given membrane (scale bar = 10 μm). In the graphs *E* and *G* the X_{Ch} is indicated by appropriate symbols. (*E*) Variation of the relative fluorescence intensity I_r as a function of the angle clockwise around the contour of the vesicle for the four different cholesterol ratios. (*F*) Order parameter, *S*, determined from the variation of the fluorescence intensity curves plotted in *E*. (*G*) Cumulative lifetime histograms $g(\tau)$ obtained from different GUV membrane compositions. (*H*) Mean fluorescence lifetimes τ obtained from the lifetime histograms $g(\tau)$ plotted as a function of the mole fraction of cholesterol in the bilayer.

cholesterol molar fractions analyzed. As expected, the data are well fitted by Eq. 1 confirming that the variation of intensity reflects the orientation of the probe in the membrane. Moreover, the data analysis quantifies the visual impression from the bottom row of Fig. 2, *A–D*, inasmuch that the restriction on the orientation distribution of the probe increases with the concentration of cholesterol in the membrane. This is further confirmed by the variation of the order parameter shown in Fig. 2 *F*. Each of the data points is the average value from at least five different vesicles. Within the range explored here the order parameter increases linearly with the cholesterol content, according to $S = 0.15 + 0.74\,X_{Ch}$.

The evolution of the probe environment as a function of X_{Ch} was further studied by analyzing the distribution of fluorescence lifetimes. The fluorescence signal coming from the bilayer in the case of the binary lipid mixtures is homogeneous and uniform. This is seen clearly in the first micrograph with GUVs containing only DOPC (Fig. 2 *A*). Due to the presence of a single fluorophore in our samples, we used a mono-exponential fit at all the relevant pixels in a micrograph to determine the fluorescence lifetime in selected areas of the membrane. The histograms are then fitted with Gaussian curves providing an average value for the fluorescence lifetimes and their distribution width. Fig. 2 *G* shows the lifetime distribution for the four DOPC/Chol membrane mixtures studied in this case. Each distribution curve is the average obtained from up to 25 measurements at each X_{Ch}. The mean lifetime values and the corresponding Gaussian widths are displayed in Fig. 2 *H*. Similar to the trends exhibited by the order parameter, the lifetimes also display a linear increase with increasing cholesterol concentration, with a best fit according to $\tau = (6.2 + 4.35\,X_{Ch})$ ns.

A parallel study was carried out with SM-containing GUVs with different cholesterol ratios. The corresponding results are shown in Fig. 3. Typical FLIM intensity images of the GUV equatorial plane are shown for each of the four membrane mixtures studied in Fig. 3, *A–D*. (X_{Ch} = 0.05, 0.13, 0.23, and 0.42). The corresponding measurements were

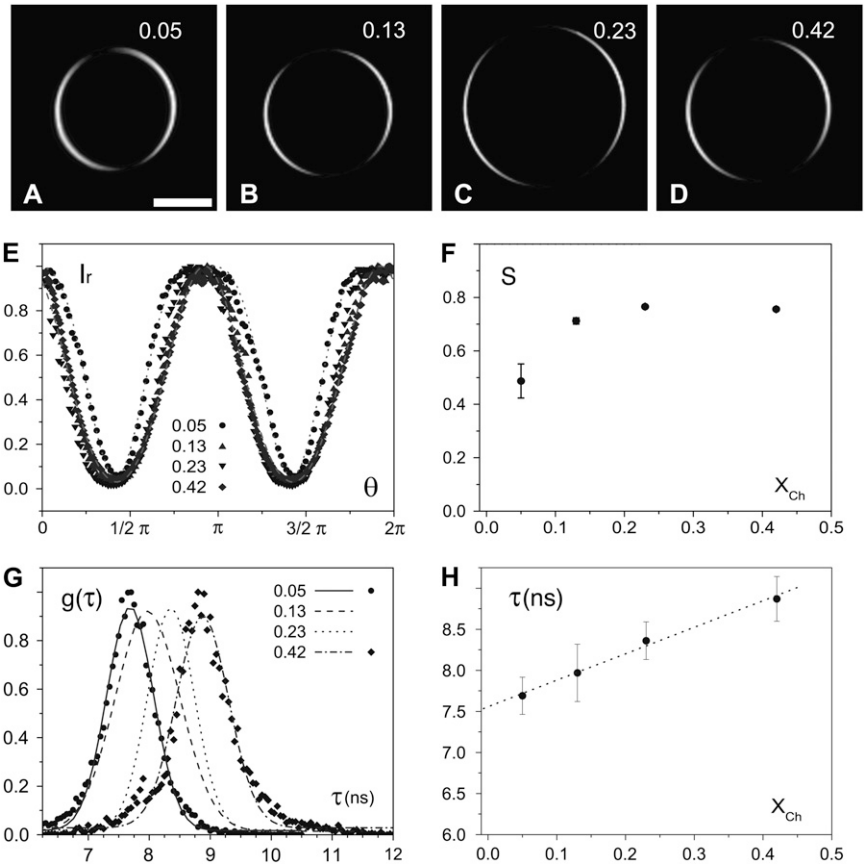

FIGURE 3 (*A–D*) FLIM intensity images representative of GUVs made from binary mixtures of SM and cholesterol (scale bar = 10 μm). The numbers refer to the mole fraction of cholesterol (X_{Ch}) in a given membrane. In graphs *E* and *G* X_{Ch} is indicated by appropriate symbols. (*E*) Variation of the relative fluorescence intensity I_r as a function of the angle clockwise around the contour of the vesicle for the four different cholesterol ratios. (*F*) Order parameter, *S*, determined from the variation of fluorescence intensity plotted in *E*. (*G*) Cumulative lifetime histograms $g(\tau)$ obtained from different GUV membrane compositions. (*H*) Mean fluorescence lifetimes τ obtained from the lifetime histograms $g(\tau)$ plotted as a function of the mole fraction of cholesterol, X_{Ch}, in the membrane.

made on at least 10 vesicles for each lipid mixture. For practical reasons related to giant vesicle formation using only gel phase lipids, the minimum amount of cholesterol considered was $X_{Ch} = 0.05$. In contrast to DOPC-containing vesicles, we could not detect, except for the lowest cholesterol content, any significant evolution of the order parameter (Fig. 3 *F*) that always displays high values. This is indicated by the presence of black areas on the vesicle contour (Fig. 3, *A–D*) and can be concluded from the minimal values reaching approximately zero in Fig. 3 *E*. The *S* values for each of the four concentrations, determined from measurements taken from at least five vesicles, are displayed in Fig. 3 *F*. As the figure shows, the order parameter for the three mole fractions: $X_{Ch} = 0.13$, 0.23, and 0.42 has high values between 0.7 and 0.8.

As with the previous DOPC/Chol GUVs, no phase separation could be observed in the present SM/Chol GUVs. Therefore, a mono-exponential function was also used to fit the fluorescence decays to obtain the lifetime histograms. A trend similar to the one observed for the DOPC/Chol vesicles was observed in the vesicles made from SM/Chol, that is, the fluorescence lifetime of the probe increases with increasing concentration of cholesterol in the bilayer. The average lifetimes extracted from the histograms of Fig. 3 *G* are plotted in Fig. 3 *H* with a best linear fit corresponding to: $\tau = (7.56 + 3.22\ X_{Ch})$ ns.

Finally, the central part of the study concerns GUVs made from an equimolar mixture of DOPC and SM with the same molar ratios of cholesterol as in Figs. 2 and 3, *B–D*. The equatorial fluorescence intensity images for each of these molar ratios are shown in Fig. 4, *A–D*. The three samples with the lowest X_{Ch} exhibit distinct domains clearly, as shown by the localization of the fluorescence intensity in the SM-rich regions, due to the much better partitioning of LcTMA-DPH in gel or L_o phases. From analysis carried out on the FLIM images, in regions of highest intensity, it was found that the partitioning of the probe favors a liquid order phase in a ratio on the order of 10:1. This value is consistent with the work carried out earlier that found the probe to favor the gel phase as well revealing a partition coefficient $K_{f/s} = 0.12$ (21). The fourth sample with $X_{Ch} = 0.42$ presents a fluorescence distribution comparable to that of the SM/Ch binary mixtures. Fig. 4 *A* corresponds to an equimolar DOPC/SM vesicle without cholesterol ($X_{Ch} = 0$). Phase separation between fluid and gel phases has obviously occurred because several probe-enriched domains with sizes significantly smaller than the vesicle dimensions can be seen along the equator. The vesicles corresponding to Fig. 4 *B* and Fig. 4 *C* display phase separation between liquid-ordered, L_o, and liquid-disordered, L_d, domains. Contrary to the DOPC/SM vesicles containing no cholesterol, the two phases here are fully separated, the brighter L_o region showing a well-defined border with the L_d

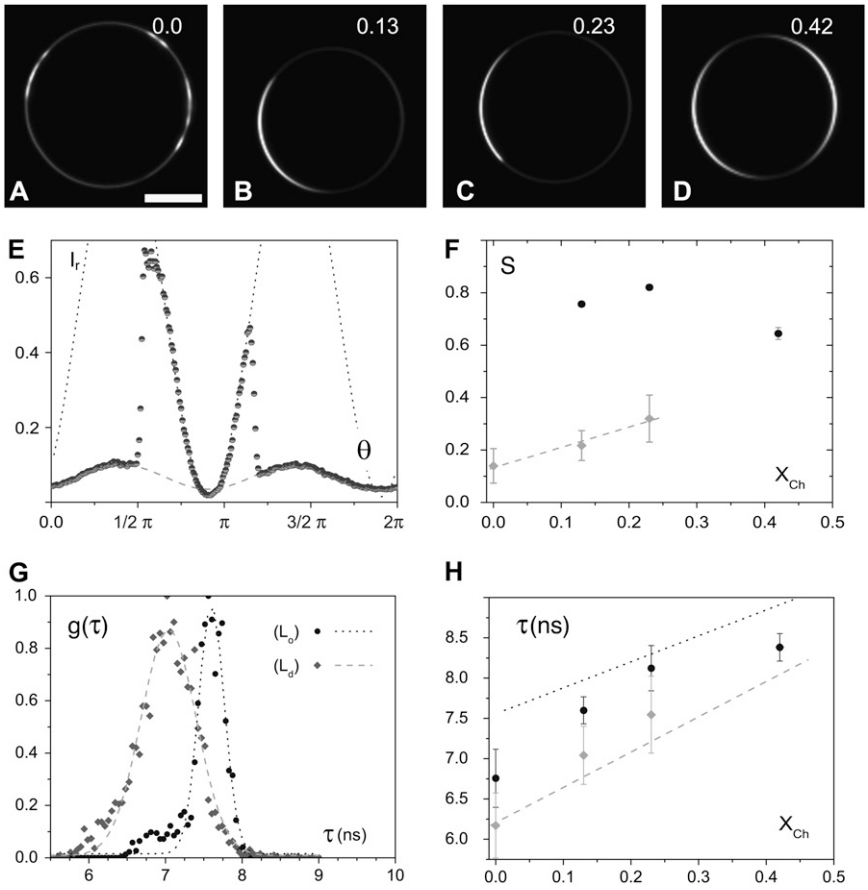

FIGURE 4 (*A–D*) Two photon FLIM intensity images representative of GUVs made from ternary mixtures of DOPC and SM (1:1 ratio), and cholesterol. The high intensity regions correspond to the SM-rich or L_o phase. The numbers refer to the mole fraction of cholesterol (X_{Ch}) in a given membrane (scale bar = 10 μm). (*E*) Variation of fluorescence intensity (●) as a function of the angle clockwise around the contour of the vesicle with $X_{Ch} = 0.23$, and the two independent sinusoidal functions used to fit the data and corresponding to the L_o (dot) and L_d (dash) separated phases. (*F*) Mean order parameter determined independently from the variation in fluorescence intensity in L_o and L_d separated phases. (*G*) Cumulative lifetime histograms obtained for the L_o (●) and L_d (◆) separated phases for vesicles with $X_{Ch} = 0.13$, and the respective gaussian fits of the data. (*H*) Mean fluorescence lifetimes for the L_o (●) and L_d (◆) phases plotted as a function of mole fraction of cholesterol in the bilayer, compared with the linear fits obtained from the corresponding data of SM/Chol (dot) or DOPC/Chol (dash) binary vesicles.

domain where the probe concentration is low. In Fig. 4 *D*, corresponding to the vesicles with the higher cholesterol ratio ($X_{Ch} = 0.42$), the phase separation is much less evident, and the whole vesicle can be considered composed of relatively homogeneous mixture of lipids.

All of these samples were analyzed by the same methods as applied to the GUVs made from binary lipid mixtures. For the vesicles presenting clear phase-separated domains, the analysis could be carried out and the information gathered separately from each of the domains, thus providing insight into the structure of the different phases (as shown in Fig. 4, *E* and *G*). In Fig. 4 *E*, it is shown clearly that the independent curves can be fitted separately for either the L_o or the L_d phases, which enables us to extract the order parameters for each individual domain. The average order parameters obtained from the separated lipid phases are plotted in Fig. 4 *F*. As can be seen, the order parameter of the probe versus cholesterol ratio shows similar trends for each type of domains (L_d or L_o) as compared to the corresponding binary vesicles (DOPC/Chol or SM/Chol, respectively). More precisely, the order parameter increases with the cholesterol ratio in the DOPC-rich domains (L_d phase) whereas the order parameter remains close to $S = 0.8$ in the SM-rich domains (L_o phase). Note that the value for the order parameter of the homogeneous ternary mixture ($X_{Ch} = 0.42$) assumes an intermediate figure between the corresponding values of the DOPC/Chol and SM/Chol binary mixtures.

The analysis of the distribution of the probe fluorescence lifetimes was carried out separately in each of the visualized domains, corresponding either to the L_o or the L_d phase. As done for the vesicles of binary compositions, the fluorescence decays were again fitted by a mono-exponential function for each of the individual domains in a given GUV. Fig. 4 *G* shows the characteristic lifetime distributions for the vesicles with a cholesterol molar ratio $X_{Ch} = 0.13$. As can be seen, the lifetime histograms are well defined for each lipid phase, with mean lifetimes differing significantly from each other. The average lifetimes for each of the domain types are displayed in Fig. 4 *H* and can be compared with the lifetime behavior observed for the vesicles of binary compositions shown here as the linear fits extracted from Figs. 2 *H* and 3 *H*. For the vesicles with the higher cholesterol ratio ($X_{Ch} = 0.42$), which do not show any phase separation, only a single mean fluorescence lifetime was obtained.

DISCUSSION

Polarization analysis of the binary vesicles

The strong partitioning of this probe in favor of ordered phases precludes any looping back of the DPH fluorophore

toward the membrane interface. In addition, the fluorophore has excitation and emission dipoles that are roughly collinear with its long molecular axis (32,33). The confinement of the probe is a consequence of the steric interactions between the probe and its environment. The probe orients preferentially in the direction normal to the bilayer, and our results confirm that the degree of orientation is a function of both the molecular structure of the lipids and the membrane composition.

If we denote the usual angles of the probe main axis with respect to the membrane normal by α (Fig. 5, *A–C*), and φ, which is the angle of rotation around the main axis (normal to the membrane), the equilibrium probability distribution of the probe orientation by $g(\alpha, \varphi)$, and the potential energy of the probe by $U(\alpha, \varphi)$, one has $g(\alpha, \varphi) \approx \exp(-U(\alpha, \varphi)/k_BT)$, where k_B is the Boltzmann constant and T the absolute temperature. In the absence of an average nonzero tilt of the molecules, the distribution displays a cylindrical symmetry with respect to the normal, and therefore both the potential energy and the probability distribution can be expressed as $U(\alpha,\varphi) = U(\alpha)$ and $g(\alpha,\varphi) = g(\alpha)$, respectively. Several interaction models for the potential energy can be proposed to quantify the degree of orientation of the probe. The three confinement models shown in Fig. 5, *A–C*, are particularly relevant for our work. We show in Fig. 5, *A–C*, the shapes of these confinement potentials and in Fig. 5, *D–F*, the corresponding probability distributions.

The simplest potential shape often invoked for describing the confinement effects of probe orientation is the so-called ''cone-model'' (29). The probe orientation is for this potential free to move up to some cutoff angle α_0, $U(\alpha) = 0$ for $\alpha \leq \alpha_0$ and $U(\alpha) = \infty$ for $\alpha > \alpha_0$. The distribution is therefore flat up to the cutoff angle α_0 and vanishes above it. The values of the order parameters S and P can be computed easily from this model, $S = 1/2\ (1 + \cos\alpha_0)\cos\alpha_0$ and $P = 1/8\ (1 + \cos\alpha_0)\ (7\cos^2\alpha_0 - 3)\cos\alpha_0$. An illustrative $[P,S]$ diagram is shown in Fig. 6 *A*, where the parametric curve $(P(\alpha_0),S(\alpha_0))$ is displayed. As the figure shows, the parametric curve of the cone-model (*dashed line*) describes the experimental S and P values reasonably well for the binary system DOPC/Chol. Because we have determined (Fig. 2 *F*) that the order parameter follows a linear dependence with the cholesterol concentration in this system, $S = 0.15 + 0.74\ X_{Ch}$, we can compute the effect of X_{Ch} on the confinement angle α_0 by solving the implicit equation, $S(X_{Ch}) = S(\alpha_0)$. Fig. 6 *B* shows the resulting curve $\alpha_0(X_{Ch})$. As expected, the larger cone angle, of roughly $\alpha_0 = 0.39\ \pi$ radians corresponds to the pure DOPC system that does not confine the probe, whereas the strongest confinement, achieved for the largest cholesterol concentration $X_{Ch} = 0.42$, corresponds to an angle $\alpha_0 = 0.28\ \pi$ radians.

A different confinement model, that we could name ''probe-on-cone'' is described by the potential and distribution shown in Fig. 5, *B* and *E*. In this model the probe retains the cylindrical symmetry with respect to the membrane normal, but is fixed at a given angle α_0. The order parameters S and P are thus simply computed from their definitions $S =$

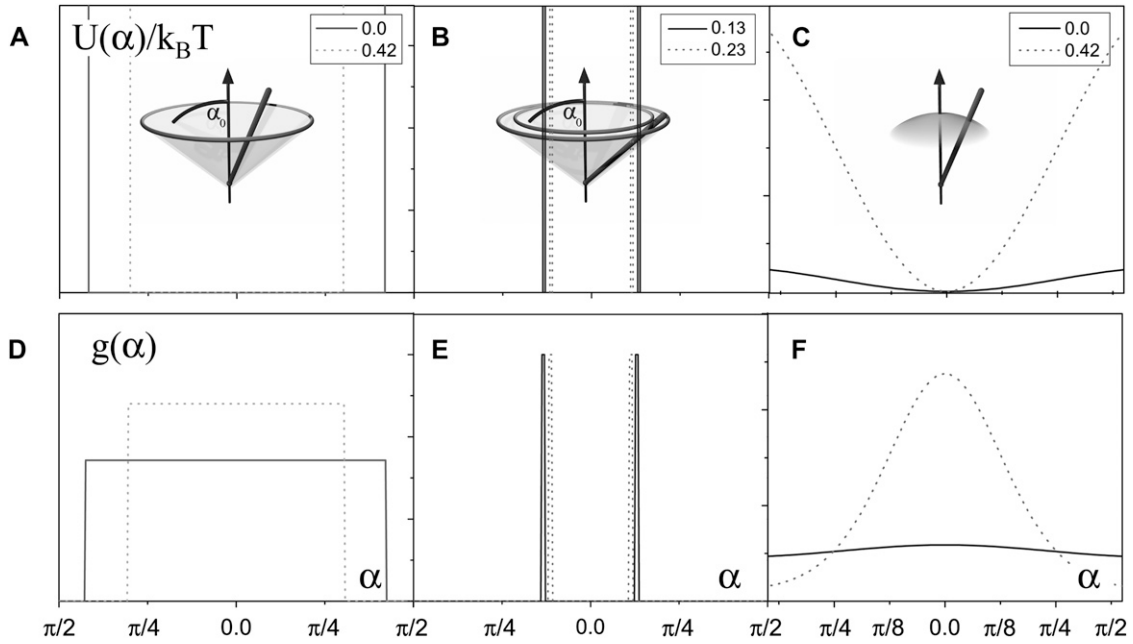

FIGURE 5 The X_{Ch} values for which the model function was calculated are indicated in all of the figures. (*A*) The cone confinement potential of the probe orientation that describes DOPC/Chol vesicles well, with a cartoon representing the free orientation of a probe up to a cut-off angle α_0 for the potential $U(\alpha)$. (*B*) The ''probe-on-cone'' confinement potential where the probe retains cylindrical symmetry, but has a fixed angle α_0 with respect to the membrane normal, a model that describes the liquid order domains of the ternary vesicles well, and to some extent the binary SM/Chol mixtures. (*C*) The parabolic confinement potential $U(\alpha) = k\ (1 - \cos^2(\alpha))$, a potential appropriate to describe liquid disordered domains of the ternary vesicles. (*D–F*) Corresponding probability distributions as a function of angle (α) for different samples for the mole fractions of cholesterol indicated.

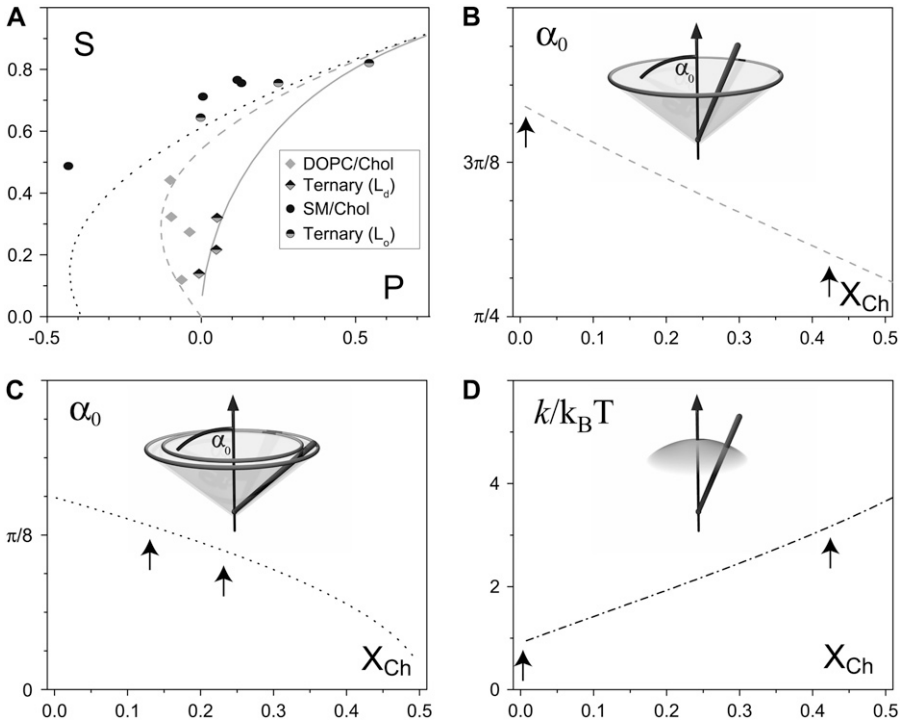

FIGURE 6 (*A*) [*P*,*S*] diagram showing the *S*(*P*) curves for each of the three models discussed in Fig. 5; ''probe on a cone'' (*dotted line*), cone confinement (*dashed line*), and parabolic confinement (*solid line*). The experimentally determined *S*(*P*) values are also shown as individual points in this diagram. (*B*) The cone angle α_0 as a function of X_{Ch} in the bilayer, for the binary system DOPC/Chol. The cartoons are a reminder of the type of confinement membrane potential that was introduced in Fig. 5 to describe the data. The arrows indicate the composition and confinement angle for the samples represented in Fig. 5, *A* and *D*. (*C*) The cone angle α_0 as a function of X_{Ch} in the bilayer, for the liquid order domains in the ternary vesicles, the arrows also indicate the samples represented in Fig 5, *B* and *E*. (*D*) The confinement strength of the parabolic potential that adequately describes the liquid disorder domains in the ternary vesicles, and the positions of the samples of Fig. 5, *C* and *F*.

$S(\alpha = \alpha_0)$ and $P = P(\alpha = \alpha_0)$. The corresponding curve *S(P)* is also plotted in Fig. 6 *A* (*dotted line*). As the figure shows, the curve from the ''probe-on-cone'' model is the one that represents data from the liquid ordered (L_o) domains of the ternary mixtures more accurately. Assuming a linear variation of the order parameter, *S*, with cholesterol content in the L_o domains of the ternary systems, as depicted in Fig. 4 *F*, $S = 0.67 + 0.65\ X_{Ch}$, we can invert the implicit equation $S(X_{Ch}) = S(\alpha_0)$ and plot the variation $\alpha_0(X_{Ch})$ of the cone angle α_0 as a function of cholesterol content X_{Ch} in Fig. 6 *C*. Note that the line has a significance only where liquid order domains exist. The angle that the probe makes with the membrane normal appears, in this case, to be close to 0.11π radians. Values for the cholesterol content, $X_{Ch} = 0.13$ and $X_{Ch} = 0.23$, were chosen to make a realistic representation of the confinement potentials displayed in Fig. 5, *B* and *E*.

In general, a function of the natural variable $\cos(\alpha)$ that obeys at the lowest order to the symmetry of the problem is $U(\alpha) = k\,(1 - \cos^2(\alpha))$. The constant *k* expresses the strength of the confinement potential. Note that close to $\alpha = 0$ one has $U(\alpha) = k\,\alpha^2$ and *k* is thus related to the magnitude of angle fluctuations $\langle\alpha^2\rangle = k_BT/(2\,k)$. Fig. 5, *C* and *F*, show the shape of the potential $U(\alpha)$ and of the corresponding normalized distribution $g(\alpha)$ for two different values of *k*. The *S*(*P*) representation on Fig. 6 *A* (*solid line*) shows that the confinement of the probe in the liquid-disordered domains of the ternary phase seem to be well represented by such potential. From the linear dependence of the order parameter with the cholesterol concentration in $S = 0.13 + 0.78\ X_{Ch}$ shown in Fig. 4 *F*, we can compute the effect of X_{Ch} on the confinement strength *k* by solving the implicit equation, $S(X_{Ch}) = S(k)$. The resulting $k(X_{Ch})$ curve is shown in Fig. 6 *D*. In the absence of cholesterol, the effect of confinement is minimal, *k* is only a limited fraction of k_BT, the thermal energy unit. As the cholesterol content is increased the confinement strength increases almost linearly to reach $k = 3\ k_BT$ for the highest cholesterol content, $X_{Ch} = 0.42$. Note that variations of this parabolic confinement potential, of the type $U(\alpha) = k\ (1 - \cos^2(\alpha))^n$ can be used to interpolate between parabolic confinement and the cone model, which is formally obtained in the limit $n \rightarrow \infty$. *S*(*P*) curves for finite *n* lie in the space between the $n = 2$ and $n \rightarrow \infty$ limits.

The experimental analysis of the intensity distribution for the SM/Ch binary mixtures in Fig. 3 shows that the probe is very well oriented for all the cholesterol concentrations, albeit with a value of the order parameter slightly smaller for $X_{Ch} = 0.05$. The ''probe-on-cone'' model seems to be the closest to the experimental data from these binary mixtures, except for the case $X_{Ch} = 0.05$ that lies far from any of the curves in Fig. 6 *A*. This smaller cholesterol concentration $X_{Ch} = 0.05$ is reportedly in a two-phase region, where a gel SM phase coexists with a minor liquid ordered phase (34). We do not see any evidence for phase separation on the optical length scale, but the difference in *S* from those vesicles with cholesterol concentrations above $X_{Ch} = 0.13$ values suggests that the system has a very different membrane structure. It is also worth noting that the SM/Ch and the DOPC/Ch polarization curves exhibit no noticeable phase shift, within accuracy of our measurements, and therefore indicates that the presence of cholesterol does not induce any average, noncylindrically symmetric tilt in the orientation of the lipids.

We can conclude from the studies of variations of the order parameter in the binary and ternary mixtures, that the polarization analysis of the LcTMA-DPH probe is particularly useful for investigating DOPC-rich regions in the phase diagram. As we will now discuss, this method provides complementary information to the analysis of the fluorescence lifetime of the probe.

Lifetime analysis of the binary vesicles

The measure of fluorescence lifetimes for the DOPC/Ch binary vesicles showed a consistent increase of the average lifetime, in the range of 6–8 ns, with increasing cholesterol ratio in the bilayer. Such an increase is usually explained as a consequence of the increase in viscosity of the DOPC phase on addition of cholesterol (35). An interesting feature of the data collected here is that the variation is linear with X_{Ch}, and therefore allows for an easy calibration of the cholesterol content of a domain with unknown composition based on mean fluorescence lifetime determined from our measurements. Note that from this perspective, lifetime measurements with our probe in DOPC-rich membranes are less sensitive to the cholesterol content than polarization measurements. Indeed, the value of the order parameter increases by a factor three for the systems studied here, whereas the corresponding lifetime increase is only 30%.

The SM/Ch binary vesicles display a similar variation of the lifetime with cholesterol content because the fluorescence lifetime of the probe, τ, increases by 20% in the experimental range (7.2–8.6 ns) spanned by our samples. The linear behavior of $\tau(X_{Ch})$ also allows for an easy calibration of samples with unknown cholesterol content. If we recall that for these mixtures the order parameter is insensitive to cholesterol content, we conclude that lifetime measurements are well suited to study the SM-rich zones of the phase diagram. Thus, the type of lipid used in this study affects both the partitioning behavior and the fluorescence lifetime of the probes. SM-rich domains exhibit a greater increase in lifetime when compared to DOPC rich domains. Moreover, it can be seen from the consistent linear trends displayed in Figs. 2 *H* and 3 *H*, that the probe is sensitive to the packing of the lipid membrane, and that in turn, reflects sensitivity to the presence of cholesterol, independent of the type of phospholipid used.

A recent FLIM study on GUVs composed of ternary mixtures of DPPC, DOPC, and cholesterol using Rhod-DOPE as a probe, also shows an effect of cholesterol concentration on the fluorescence lifetime. In that study the fluorescence lifetime *decreases* with increasing cholesterol concentration (17). This is most likely due to the differences between the photophysical properties of fluorophores, and the effect of the surroundings on the lifetimes of the different probes used in that study and the one used in this study. Rhod-DOPE, which is a headgroup-labeled phospholipid is most likely at the interface between the membrane and water, whereas in our case the DPH fluorophore is deeply embedded in the membrane (i.e., in the hydrophobic core of the membrane). With the probe residing in the hydrophobic core of the lipid bilayer, the change in fluorescence lifetime reflects the changes of the inner membrane composition (i.e., the addition of cholesterol to the bilayer or the presence of lipids with different molecular structure of their acyl chains).

Polarization and lifetime analysis of the ternary vesicles

The combination of polarization and lifetime analysis has shown to be a powerful tool to investigate the GUVs of binary lipid composition. Applying this approach to vesicles of ternary composition, we were able to determine both the order parameter and fluorescence lifetime in phase separated vesicles. This was made possible by analyzing the micrometer-sized domains independently (Fig. 4).

For the DOPC/SM vesicles without cholesterol, the size of the DOPC-rich domains in the membrane were large enough to accurately determine both the order parameter and the mean lifetime values. From the data analysis, the DOPC-rich domains present a structure similar to pure DOPC vesicles, as reflected by trends of the order parameter (Fig. 4 *F*) and the mean fluorescence lifetime (Fig. 4 *H*). On the other hand, and despite their small size, an average lifetime can also be extracted from the SM-rich domains as shown in Fig. 4 *H*. Contrary to the DOPC-rich domains, the SM-rich domains display lifetimes significantly smaller than those determined from the binary SM/Ch vesicles, suggesting the presence of some amount of DOPC molecules in the SM-rich domains, enough to significantly affect the membrane properties and the mean fluorescence lifetime.

For the vesicles containing cholesterol, at $X_{Ch} = 0.13$ and $X_{Ch} = 0.23$, that present well-defined L_o and L_d phase-separated domains, the order parameters measured in the phase separated domains were nearly identical. For the L_d domains this shows that the lines of constant order parameter follow a nontrivial trajectory in the ternary phase diagram. Indeed, the tie lines of the central phase-separated region are believed to be inclined with a positive slope. This means that the composition of the DOPC-rich domains contains less cholesterol than the average composition. Therefore the lines of constant order parameter, S, follow a downward path from the left border of the ternary diagram.

The average lifetimes extracted from the L_o and the L_d domains show that the local environment of the probe is significantly different from the GUVs made from a two component mixture, either SM/Ch or DOPC/Ch. In the case of L_d domains of ternary vesicles, the lifetimes (τ) are systematically above (Fig. 4 *H*) the lifetimes of the binary vesicles with the same cholesterol content. This implies that SM contributes to the average lifetime measured in the L_d domains to some extent. In an opposite way, in the case of L_o domains, the lifetimes are systematically below the lifetimes

of the corresponding binary vesicles at corresponding cholesterol content. Likewise, this implies that DOPC also contributes to the mean lifetime in the SM-rich domains. These findings are consistent with the information that can be determined from the boundaries of the two-phase region in the ternary diagram.

Thus the analysis of FLIM images, with respect to both lifetime and polarization data, provides useful information about the composition, and phase behavior of the lipids in the domains of the membrane. The determination of the probe order parameter is a powerful tool to show changes in DOPC/Ch (L_d phases), whereas changes in SM/Chol (L_o phases) can be better investigated by measuring the fluorescence lifetime. Together they confirm that phase separation does not imply complete demixing of SM and DOPC in phase-separated vesicles.

APPENDIX

In our experimental configuration, where only the excited light is polarized, the light is collected from all probe orientations. This implies that each excited probe contributes equally to the intensity measured at the detector. For any given probe located on the equatorial section of the membrane at angle θ with respect to the polarization axis, the emitted light amplitude is proportional to the two-photon projection of the polarization direction on the probe tensor (36). For the probe DPH, the diagonalized tensor has only one significant diagonal value, indicating the rod like structure of the probe. In this case the emitted intensity is proportional to the fourth power of the projection of T, the unit vector associated with the probe orientation on the polarization axis, giving $I(\theta) \sim T^4$. If we denote by α and φ, the probe angles with respect to the normal to the membrane, then $T = \sin\alpha\sin\varphi\sin\theta + \cos\alpha\cos\theta$. Moreover if $g(\alpha,\varphi)$ is the corresponding equilibrium distribution, one has the following expression for the intensity:

$$I(\theta) = 1/(4\pi)\int_0^{2\pi} d\varphi \int_0^{\pi} d\alpha \sin\alpha \left(\sin\alpha\sin\varphi\sin\theta + \cos\alpha\cos\theta\right)^4 \times g(\alpha,\varphi). \quad \text{(A1)}$$

If we further assume an isotropic distribution $g(\alpha,\varphi) = g(\alpha)$, then one gets the expression:

$$I(\theta) = (1/5 - 2S/7 + 3P/35 + 6(S-P)/7\sin^2(\theta) + P\sin^4(\theta)) \quad \text{(A2)}$$

with the order parameters $S = \langle(3\cos^2\alpha - 1)/2\rangle$, and $P = \langle(3 - 30\cos(\alpha)^2 + 35\cos(\alpha)^4)/8\rangle$ that are computed by averaging $\langle\ \rangle$ the Legendre functions of second and fourth order over the equilibrium distribution $g(\alpha)$. Note that this assumes that the incident light in the two-photon confocal volume has a well-defined polarization perpendicular to the microscope axis. Due to optical effects related to the different optical elements of the microscope, this is known to be only approximately true, and therefore small polarization components may exist in the other two orthogonal directions. Our analysis neglects such corrections.

We thank J.P. Clamme for the assistance with initial FLIM measurements and the demonstration of the data analysis software. C.M. acknowledges insightful discussions with F. Thalmann. C.H. thanks the Laboratoire European Associé ''Macromolecules et Milieux Divisés'' for a post-doctoral grant.

REFERENCES

1. Kahya, N., D. Scherfeld, K. Bacia, B. Poolman, and P. Schwille. 2003. Probing lipid mobility of raft-exhibiting model membranes by fluorescence correlation spectroscopy. *J. Biol. Chem.* 278:28109–28115.
2. Dietrich, C., L. A. Bagatolli, Z. N. Volovyk, N. L. Thompson, M. Levi, K. Jacobson, and E. Gratton. 2001. Lipid rafts reconstituted in model membranes. *Biophys. J.* 80:1417–1428.
3. Brown, D. A., and E. London. 2000. Structure and function of sphingolipid- and cholesterol-rich membrane rafts. *J. Biol. Chem.* 275: 17221–17224.
4. Simons, K., and E. Ikonen. 1997. Functional rafts in cell membranes. *Nature.* 387:569–572.
5. Edidin, M. 2003. The state of lipid rafts: from model membranes to cells. *Annu. Rev. Biophys. Biomol. Struct.* 32:257–283.
6. Feigenson, G. W. 2007. Phase boundaries and biological membranes. *Annu. Rev. Biophys. Biomol. Struct.* 36:63–67.
7. Baumgart, T., S. T. Hess, and W. W. Webb. 2003. Imaging coexisting fluid domains in biomembrane models coupling curvature and line tension. *Nature.* 425:821–824.
8. Lagerholm, B. C., G. E. Weinreb, K. Jacobson, and N. L. Thompson. 2005. Detecting microdomains in intact cell membranes. *Annu. Rev. Phys. Chem.* 56:309–336.
9. Klausner, R. D., and D. E. Wolf. 1980. Selectivity of fluorescent lipid analogues for lipid domains. *Biochemistry.* 19:6199–6203.
10. Loura, L. M., A. Fedorov, and M. Prieto. 2000. Partition of membrane probes in a gel/fluid two-component lipid system: a fluorescence resonance energy transfer study. *Biochim. Biophys. Acta.* 1467:101–112.
11. Baumgart, T., G. Hunt, E. R. Farkas, W. W. Webb, and G. W. Feigenson. 2007. Fluorescence probe partitioning between Lo/Ld phases in lipid membranes. *Biochim. Biophys. Acta.* 1768:2182–2194.
12. Feigenson, G. W. 2006. Phase behavior of lipid mixtures. *Nat. Chem. Biol.* 2:560–563.
13. Veatch, S. L., I. V. Polozov, K. Gawrisch, and S. L. Keller. 2004. Liquid domains in vesicles investigated by NMR and fluorescence microscopy. *Biophys. J.* 86:2910–2922.
14. Veatch, S. L., and S. L. Keller. 2005. Miscibility phase diagrams of giant vesicles containing sphingomyelin. *Phys. Rev. Lett.* 94:148101.
15. Xu, X., and E. London. 2000. The effect of sterol structure on membrane lipid domains reveals how cholesterol can induce lipid domain formation. *Biochemistry.* 39:843–849.
16. Bagatolli, L. A., and E. Gratton. 2000. A correlation between lipid domain shape and binary phospholipid mixture composition in free standing bilayers. *Biophys. J.* 79:434–447.
17. de Almeida, R. F., J. Borst, A. Fedorov, M. Prieto, and A. J. Visser. 2007. Complexity of lipid domains and rafts in giant unilamellar vesicles revealed by combining imaging and microscopic and macroscopic time-resolved fluorescence. *Biophys. J.* 93:539–553.
18. Ariola, F. S., D. J. Mudaliar, R. P. Walvick, and A. A. Heikal. 2006. Dynamics imaging of lipid phases and lipid-marker interactions in model biomembranes. *Phys. Chem. Chem. Phys.* 8:4517–4529.
19. Azoulay, J., J. P. Clamme, J.-L. Darlix, B. P. Roques, and Y. Mély. 2003. Destabilization of the HIV-1 complementary sequence of TAR by the nucleocapsid protein through activation of conformational fluctuations. *J. Mol. Biol.* 362:691–700.
20. Margineanu, A., J. Hotta, R. A. Vallee, M. Van der Auweraer, M. Ameloot, A. Stefan, D. Beljonne, Y. Engelborghs, A. Herrmann, K. Mullen, F. C. De Schryver, and J. Hofkens. 2007. Visualization of membrane rafts using a perylene mono imide derivative and fluorescence lifetime imaging. *Biophys. J.* 93:2877–2891.
21. Beck, A., D. Heissler, and G. Duportail. 1993. Influence of the length of the spacer on the partitioning properties of amphiphilic fluorescent membrane probes. *Chem. Phys. Lipids.* 66:135–142.
22. Xu, X., R. Bittman, G. Duportail, D. Heissler, C. Vilcheze, and E. London. 2001. Effect of the structure of natural sterols and sphingolipids on the formation of ordered sphingolipid/sterol domains (rafts).

Comparison of cholesterol to plant, fungal, and disease-associated sterols and comparison of sphingomyelin, cerebrosides, and ceramide. *J. Biol. Chem.* 276:33540–33546.

23. Bakht, O., P. Pathak, and E. London. 2007. Effect of the structure of lipids favoring disordered domain formation on the stability of cholesterol-containing ordered domains (lipid rafts): identification of multiple raft-stabilization mechanisms. *Biophys. J.* 93:4307–4318.
24. Beck, A., D. Heissler, and G. Duportail. 1993. 1,1-Thionyldi-imidazole in the synthesis of a long-chain phospholipid membrane probe. *J. Chem. Soc. Chem. Commun.* 31–32.
25. Dimitrov, D. S., and M. I. Angelova. 1987. Electric field mediated lipid swelling and liposome formation. *Stud. Biophys.* 119:61–65.
26. Clamme, J. P., J. Azoulay, and Y. Mély. 2003. Monitoring of the formation and dissociation of polyethylenimine/DNA complexes by two photon fluorescence correlation spectroscopy. *Biophys. J.* 84:1960–1968.
27. Korlach, J., P. Schwille, W. W. Webb, and G. W. Feigenson. 1999. Characterization of lipid bilayer phases by confocal microscopy and fluorescence correlation spectroscopy. *Proc. Natl. Acad. Sci. USA.* 96:8461–8466.
28. Florine-Casteel, K., J. J. Lemasters, and B. Herman. 1991. Lipid order in hepatocyte plasma membrane blebs during ATP depletion measured by digitized video. *FASEB J.* 5:2078–2084.
29. Kinosita, K., S. Kawato, and A. Ikegami. 1977. A theory of fluorescence polarization decay in membranes. *Biophys. J.* 20:289–305.
30. Florine-Casteel, K. 1990. Phospholipid order in gel-and fluid-phase cell-size liposomes measured by digitized video. *Biophys. J.* 57:1199–1215.
31. Shinitzky, M. 1972. Effect of fluorescence polarization on fluorescence intensity and decay measurements. *J. Chem. Phys.* 56:5979–5981.
32. Engel, L. W., and F. G. Prendergast. 1981. Values for and significance of order parameters and ''cone angles'' of fluorophore rotation in lipid bilayers. *Biochemistry.* 20:7338–7345.
33. Lentz, B. R. 1989. Membrane ''fluidity'' as detected by diphenylhexatriene probes. *Chem. Phys. Lipids.* 50:171–190.
34. de Almeida, R. F. M., A. Fedorov, and M. Prieto. 2003. Sphingomyelin/ phosphatidylcholine/ cholesterol phase diagram: boundaries and composition of lipid rafts. *Biophys. J.* 85:2406–2416.
35. Kalb, E., F. Paltauf, and A. Hermetter. 1989. Fluorescence lifetime distributions of diphenylhexatriene-labeled phosphatidylcholine as a tool for the study of phospholipid-cholesterol interactions. *Biophys. J.* 56:1245–1253.
36. Callis, P. R. 1997. The theory of two-photon induced fluorescence anisotropy. J. R. Lakowicz, editor. Plenum Publishing, New York. 1–42.